Published in final edited form as:
ACS Photonics. 2018 ; 5(3): 955–963. doi:10.1021/acsphotonics.7b01231.

High Internal Quantum Efficiency Ultraviolet Emission from Phase-Transition Cubic GaN Integrated on Nanopatterned Si(100)

Richard Liu[†,‡], **Richard Schaller**[§], **Chang Qiang Chen**[‖], and **Can Bayram**[*,†,‡]

[†]Department of Electrical and Computer Engineering, University of Illinois at Urbana–Champaign, Urbana, Illinois 61801, United States

[‡]Micro and Nanotechnology Technology Laboratory, Urbana, Illinois 61801, United States

[§]Center for Nanoscale Materials, Argonne National Laboratory, Argonne, Illinois 60439, United States

[‖]Frederick Seitz Materials Research Laboratory, University of Illinois at Urbana–Champaign, Urbana, Illinois 61801, United States

Abstract

Ultraviolet emission characteristics of cubic (c-) GaN enabled through hexagonal-to-cubic phase transition are reported. Substrate patterning and material growth are shown to affect phase purity and emission characteristics of c-GaN as studied by electron backscatter diffraction, and photo- and cathodoluminescence, respectively. Raman study shows a tensile strain in the c-GaN. Time-resolved photoluminescence reveals c-GaN band edge emission decay time of 11 ps. The ultraviolet emissions from both phases of GaN are linearly polarized in the same direction, which is along the $\langle 11\bar{2}0\rangle$ and $\langle 110\rangle$ directions of hexagonal GaN and c-GaN, respectively. Temperature-dependent (5.7 to 280 K) cathodoluminescence studies reveal an internal quantum efficiency of ~29% at room temperature along with intrinsic and extrinsic defect energy levels of ~124 and ~344 meV, respectively, of the phase-transition c-GaN. Using the IQE value and carrier decay lifetime, a radiative lifetime of 38 ps is extracted. Overall, photonic properties of phase-transition c-GaN and their dependence on substrate patterning and material growth are reported.

Graphical Abstract

[*]**Corresponding Author:** cbayram@illinois.edu.

The authors declare no competing financial interest.

ASSOCIATED CONTENT

Supporting Information

The Supporting Information is available free of charge on the ACS Publications website at DOI: 10.1021/acsphotonics.7b01231. Temperature-dependent photoluminescence spectra of conventional 3-μm-thick h-GaN on sapphire; temperature-dependent photoluminescence spectra of HVPE-grown 325-μm-thick freestanding h-GaN; temperature-dependent photoluminescence spectra of h-GaN on Si(111) (PDF)

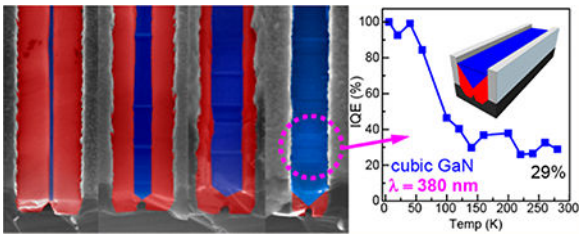

Keywords

cubic phase; gallium nitride; cathodoluminescence; electron backscatter diffraction; photoluminescence; ultraviolet emitter

Gallium nitride (GaN) and its alloys are the semiconductors of choice for driving the solid-state lighting revolution through the white light emitting diodes (LEDs).[1] Such LEDs are hexagonal (wurtzite) phase semiconductors and conventionally grown on the polar (0001) plane of the thermodynamically stable hexagonal (h-) phase of GaN. However, the lack of inversion symmetry in h-crystal structure leads to strong spontaneous and piezoelectric polarization fields (~MV/cm) along the ⟨0001⟩ growth direction. Such large electric fields have many detrimental effects in photonics (reducing the radiative recombination rates in LEDs due to the quantum confined Stark effect[2]) and electronics (dictating a normally on operation in high electron mobility transistors, HEMTs[3]).

As such, unconventional crystal facets such as the nonpolar $(1\bar{1}00)$ m-plane of h-GaN with zero polarization fields are being explored. However, these substrates suffer from low availability, low scalability, and high defectivity.[4–6] This necessitates the search for novel GaN photonic materials with zero polarization nature and yet on an inexpensive, scalable platform.

GaN also forms in the cubic (zincblende) phase. The cubic phase of GaN (c-GaN) is inherently polarization-free in the ⟨100⟩ growth direction due to its centrosymmetric atomic arrangement.[7] Additionally, c-GaN has benefits such as high carrier mobility,[8] high p-type conductivity,[9] high electron drift velocity,[10] small Auger losses,[11] high optical gain,[12] high radiative efficiency,[13,14] and cleavage planes.

Most notably, the band gap of c-GaN (E_g = 3.22 eV) is 0.2 eV smaller than that of h-GaN (E_g = 3.42 eV). The conventional high-indium-content h-InGaN green LED is 4 times less efficient than the blue and red LEDs; this creates the so-called “green gap”, as the available semiconductors cannot emit in this part of the spectrum efficiently.[15] To date, the green gap has prohibited the implementation of full spectrum solid-state LEDs for display and lighting applications. This makes cubic III-nitrides an exciting material for addressing the green gap in the visible spectrum, as less (~10%) indium content is needed in green-emitting cubic InGaN multiquantum wells.[16]

The most important issue hampering c-GaN is its metastability when grown directly on conventional cubic substrates (MgO,[17] GaAs,[18] 3C-SiC[19]), limiting its practicality. GaN

grown via such an approach results in highly defective (>10^{10} cm^{-2}) and mixed h-/c-phase materials, as GaN thermodynamically prefers the h-GaN crystal formation.[20]

An alternative approach, hexagonal-to-cubic phase transition, has recently been introduced to synthesize single-crystalline stable c-GaN.[21–23] Here we employ this approach to enable high phase purity and high crystal quality c-GaN via metalorganic chemical vapor deposition (MOCVD) on a CMOS-compatible on-axis nanopatterned Si(100) substrate.[24] By meeting critical substrate patterning and growth conditions, we circumvent the need for any postgrowth processing techniques (e.g., ion beam milling) to enable complete phase-transition c-GaN surface coverage.[25] Thus, our approach enables us to study and report on the structural and optical properties of the as-grown phase-transition c-GaN and demonstrate the effect of growth and patterning on the crystal quality and luminescence characteristics. In addition, our employment of Si(100) as the substrate reduces cost, increases scalability, and opens up heterointegration opportunities.

The hexagonal-to-cubic phase transition of GaN is facilitated on a U-shape nanogrooved Si(100) substrate.[24] As shown in Figure 1, the U-groove consists of two vertical dielectric sidewalls confining two opposing Si(111) planes and a Si(100) plane in the center. We recently showed that U-groove parameters, which are dielectric opening width (p), silicon etch depth (t_d), and dielectric sidewall angle (α), affect the phasetransition c-GaN surface coverage atop the U-grooves. Complete c-GaN surface coverage occurs when the deposition thickness (h) of GaN deposited above the Si(100) substrate surface equals the critical thickness (h_c):[25]

$$h_c = \frac{1.06p - 0.75t_d}{1 - \tan\alpha/0.71} \quad (1)$$

RESULTS

Three different c-GaN surface coverage outcomes (complete, underdeposition, overdeposition) are schematically presented in Figure 1a,c,e, and their representative cross-sectional scanning electron microscopy (SEM) images are shown in Figure 1b,d,f. In the U-grooves, h-GaN (colored red) nucleates on the (111) planes of the silicon substrate, making an angle of 54.7° to the Si(100) plane. The two opposing h-GaN wings then merge at twice the angle (54.7° × 2 = 109.4°) at a seam point where phase transition from h-GaN (colored red) to cGaN (colored blue) initiates. Thus, the c-GaN (100) plane is parallel to that of the Si(100) substrate. A void forms below that seam point. Optimized growth and patterning conditions ($h = h_c$) are presented in Figure 1a,b.

The two nonideal deposition scenarios are under- and overdeposition. In the former case (Figure 1c,d) the phasetransition c-GaN does not grow over the h-GaN wings. Hence, the $(10\bar{1}1)$ planes of the h-GaN wings, making an angle of ~7° to the Si substrate, are observed. Achieving complete c-GaN coverage requires further GaN deposition, much needed to increase h to the level of h_c. In the latter case (Figure 1e,f), overgrowth above the c-GaN rhombus becomes mixed phase, which is due to h-GaN growth from the sidewalls. In order

to quantify between under-, ideal-, and overdeposition cases, we define the h/h_c ratio as the fill factor (*ff*) where an *ff* less than 100% suggests underdeposition, whereas an *ff* more than 100% suggests overdeposition.

Electron backscatter diffraction (EBSD) studies are conducted to investigate the phase transition of GaN. The Kikuchi bands formed by a 15 kV electron beam is used to distinguish the crystal phases, orientation, and grain (phase) boundaries of the GaN in U-grooves with a spatial resolution of ~50 nm. To best study the phase transition, EBSD was conducted on the undergrown sample (Figure 1c,d) with 20 nm × 20 nm pixels.

The 70° tilted view SEM image of the undergrown Ugrooves is shown in Figure 2a. The c-GaN "plateau" can be seen sandwiched between two h-GaN "wings", which are neighbored by the "SiO_2" dielectric sidewalls. The EBSD phase detection of the region marked by the red rectangle in Figure 2a is shown in Figure 2b, with red, blue, and black pixels representing hexagonal, cubic, and indistinguishable crystal phases, respectively. The inverse pole figures (IPF) of the [100], [010], and [001] directions of the same region are plotted in Figure 2e,f,g. The color indices for IPFs of c-GaN and h-GaN are provided in Figure 2c,d. It is seen that the plateau region of the U-groove is composed of solely c-GaN with no visible grain boundary and crystal misalignment. Similar to the Si(100) substrate, the c-GaN plateau has its (100) plane pointing in the normal direction and the {110} planes along and perpendicular to the grooves. These results indicate the phase transition of GaN in the U-grooves is uniform and controllable and leads to a single-crystalline c-GaN surface. These results demonstrate an opportunity for studying the optical properties of phase-transition c-GaN.

A transmission electron microscopy (TEM) study is conducted to characterize the crystal quality of the GaN materials in a U-groove, as shown in Figure 3: (a) bright field and (b) dark field images. A highly defective and thin (~15 nm) layer of AlN is seen covering the Si substrate and the amorphous oxide barriers. Near the h-GaN nucleation sites on the Si(111) planes, both TEM images show crystals containing dislocations and stacking faults. The h-GaN crystals that are more than 50 nm away from the nucleation sites show increased quality, and dislocations are rarely observed. A ~20 nm long seam oriented perpendicular to the substrate is observed in the middle of the groove between the two opposing h-GaN wings directly above the void. It terminates into two distinctly straight interfaces extending toward the oxide sidewalls to form a V-shaped boundary. Enclosed in the V-boundary is the c-GaN cubic crystal, which is further confirmed by TEM electron diffraction taken from the triangular area shown in Figure 1a. Stacking faults parallel to the interface, i.e., lying on the c-GaN (111) and h-GaN (0001) planes, are observed to accommodate the transition between the two crystal structures, but are limited to within a few layers of atoms thick (not shown). At the c-GaN/oxide interface near the surface, defects (stacking faults) are observed to orient away from the oxide (Figure 3b). Defective and mixed-phase material are observed above these stacking faults and the aforementioned critical height, h_c. This demonstrates the importance of silicon substrate patterning and GaN growth optimization, as inadvertent relaxation of c-GaN to mixed-phase material can occur at the c-GaN/barrier.

Raman spectroscopy is used to study the crystallinity and strain of GaN materials grown in various-sized U-grooves. Using a Horiba Raman confocal imaging microscope with a depolarized 405 nm laser and 1800 lines/mm grating, Raman spectra of U-grooves with *ff*'s ranging from 0% to 205% are collected and plotted in Figure 4 to demonstrate the effect of optimization on the crystal quality.

Four peaks in Figure 4a are identified as Si substrate (520 cm^{-1}), E_2^H(TO)and A_1(LO) of h-GaN (567 cm^{-1}, 733 cm^{-1}), and E_2^H or A_1(TO) of AlN (618 cm^{-1}). Zoomed-in Raman spectra of the TO-phonons are shown in Figure 4b, in which the 558 cm^{-1} peak, attributed to the E_1(TO) shift of h-GaN, is observed. Another peak at 551 cm^{-1}, attributed to TO-phonons of c-GaN, emerges as ff increases from 0% to 95%, signifying the increasing presence of c-GaN.[26] The peak at 733 cm^{-1} intensifies (Figure 4a), suggesting an involvement of the LO-phonons of c-GaN in addition to the E_1(LO) phonons of hGaN. Both peaks of c-GaN show a red-shift in their Stokes shift compared to the literature (555 and 742 cm^{-1} for TO- and LOphonons, respectively), indicating c-GaN is under a tensile strain,[26] which is in agreement with other studies on phasetransition c-GaN on Si(100).[22,23] This is due to the lattice mismatch between Si(111) and h-GaN being passed to the cGaN. At the extreme case of overdeposition (*ff* = 205%), all GaN-related Raman signals decrease in intensity and increase in their full-width at half maximum (fwhm), and the TO-phonon Raman mode of c-GaN becomes undetectable. We attribute this to the mixed-phase material on the surface in overgrowth samples.[27]

We perform time-integrated and time-resolved photoluminescence (PL) studies to investigate the luminescence lifetimes in h- and c-GaN. The luminescence lifetime can reveal the carrier loss mechanisms and quantitatively compare their rate and how suitable the material is for photonic applications. The measured PL lifetime (τ_{PL}) is related to the radiative lifetime (τ_{rad}) and nonradiative lifetimes (τ_{nr}) through

$$\tau_{PL}{}^{-1} = \tau_{nr}{}^{-1} + \tau_{rad}{}^{-1} \quad (2)$$

It is known that the radiative lifetime in semiconductors is determined by the scattering from the excitonic branch to the photonic branch of the exciton–polariton dispersion curves. Hence, the radiative lifetime for a 200 nm thick GaN film can be expressed as[28]

$$\tau_{rad} = \frac{1}{2}\left(\frac{5\pi}{3}\right)^{3/5}\left(\frac{M}{\nu_0}\right)^{2/5}\left\{\frac{\hbar^2 c^7 \alpha_p L^3}{C^4 \omega^6}\right\}^{1/5} \quad (3)$$

where M/ν_0 is the mass per unit volume of the unit cell (~3 kg m^{-3}), α_p is the polarizability (4×10^{-5}), L is the thickness of the excited layer (~200 nm), $\hbar\omega$ is the photon energy of the excitonic transition (3.42 eV), and C is the deformation potential (4 eV). This equation yields a theoretical radiative lifetime of ~470 ps for h-GaN. The corresponding radiative lifetime of c-GaN is estimated to be ~47 ps, an order of magnitude shorter than that of h-

GaN, as suggested by the literature.[13,29] This is due to the greater electron–hole wave function overlap, which results in a greater oscillator strength, in the absence of polarization fields in c-GaN.[13]

Experimentally, a time-resolved PL study is carried out with a frequency-tripled Ti:Al_2O_3 laser (λ = 266 nm) and a streak camera system with a temporal resolution of ~1 ps to investigate the carrier dynamics of phase-transition c-GaN. Figure 5 shows the PL spectrum with two speaks at 3.42 and 3.22 eV, which correspond to the free exciton transitions of h-GaN and c-GaN, respectively.[30] A time-resolved PL study of the selected spectral ranges, shown in Figure 5 as insets, shows exponential decays with lifetimes of 20 ps for 3.42 eV (h-GaN) and 11 ps for 3.22 eV (c-GaN).

Studies have shown that lateral epitaxial overgrowth h-GaN on sapphire exhibits a PL lifetime in the range of 80–210 ps at room temperature[31,32] and 530 ps for GaN grown by hydride vapor phase epitaxy (HVPE).[33] For c-GaN, studies reported an extremely short PL lifetime of ~15 ps.[34] For h-GaN, our data show an extremely fast decay compared to the high-quality material in the literature, suggesting an additional carrier loss mechanism in the U-grooves. However, the phase-transition c-GaN shows a comparable PL decay lifetime to the 1 μm thick c-GaN films on 3C-SiC, indicating a similar carrier recombination rate.[34]

Using eq 2 and a theoretical τ_{rad} of 470 ps (47 ps) for h-GaN (c-GaN), the nonradiative decay dominates the transition with a τ_{nr} of 21 ps (14 ps) for the h-GaN (c-GaN) in the U-grooves. We believe that the short radiative lifetimes of the two phases of GaN in the U-grooves are dominated by two mechanisms: material interfaces and strong oscillator strength. The stacking faults along the hexagonal-cubic phase-transition interfaces may act as nonradiative recombination centers.[35] The h-GaN–silicon and c-GaN–air interfaces may also provide another carrier loss mechanisms. On the other hand, a fast PL lifetime could also be the result of a strong radiative recombination resulting from the higher degree of confinement provided by the quasi 1D nature of the U-grooves. It has been reported that c-GaN has a significantly stronger oscillator strength with its smaller band gap and the lack of polarization fields.[13] We are conducting further studies to better understand the origins of ultrafast lifetimes in these materials.

Polarization-dependent PL can reveal the nature of the radiative recombination and the escape path of the photons from the material. The phase-transition c-GaN in the U-grooves exhibits polarization in the light emitted through either a grating-like effect[36] and/or strain-induced valence band splitting.[37] In this work, the U-grooves are orientated parallel to the passing axis of the polarizer at 0°, and the normalized result is plotted in Figure 6. The band edge emissions from h-GaN and c-GaN are shown by red squares and blue circles, respectively. The emissions from both phases of GaN are linearly polarized in the same direction, which is along the $\langle 11\bar{2}0 \rangle$ and $\langle 110 \rangle$ directions of h-GaN and c-GaN/Si, respectively. The magnitude of the polarization of the emitted photons is characterized by the degree of polarization (ρ), which is

$$\rho = \frac{I_{\parallel} - I_{\perp}}{I_{\parallel} + I_{\perp}} \quad (4)$$

where $I_{\parallel}$ and $I_{\perp}$ are the intensity when the passing axis of the polarizer is parallel and perpendicular to the U-grooves, respectively. The values are found to be 0.12 for h-GaN and 0.20 for c-GaN. The polarization of h-GaN emission (3.42 eV) in a grating-like setting has been reported to have a strong linear polarization parallel to the direction of the grating,[38] which is in good agreement with the results shown in Figure 6. The polarization observed in this work is believed to be the result of a combination of the grating effect and tensile strain, which is determined through Raman studies.

Cathodoluminescence (CL) is used to study phase purity, defect distribution, impurity levels, and internal quantum efficiencies of various GaN materials in U-grooves. Particularly, CL can map the luminescence with a spatial resolution of <1 μm, providing useful insights on the spatial distribution of the radiative recombination centers. Our study was conducted via a JEOL JSM 7000F field emission scanning electron microscope outfitted with a Gatan MonoCL3 for panchromatic/monochromatic imaging and spectroscopy with a wavelength resolution of 2 nm fwhm and a helium-flow cryo-stage capable of temperature control from 5.65 K to >300 K. The electron beam is set to emit a beam current of 0.1–3.2 nA at 2 kV, which yields a maximum electron penetration depth of ~47 nm.[39] This allows for a good combination of maximizing signal intensity while minimizing the amount of excitation of the hGaN wings buried underneath the c-GaN isosceles triangle (Figure 1a).

As shown by Raman spectroscopy and EBSD, the *ff* = 95% is the most optimized U-groove sample for c-GaN and provides the largest surface coverage of phase-transition c-GaN with the highest crystal quality. As such, a CL study conducted on this U-groove configuration reveals the optical properties of the highest quality c-GaN enabled via phase transition. Figure 7 shows the CL spectrum of the *ff* = 95% U-grooves conducted at 5.7 K with variable electron beam current in raster scan mode, which gives a good representation of the luminescence properties of the top 47 nm layer over a 20 × 30 μm^2 area.

Three luminescence centers are observed and identified as bound exciton (BX) and donor–acceptor pairs (DAP_1 and DAP_2) at 3.28, 3.17, and 2.95 eV, respectively. LO-phonons of the DAPs are also observed at energy intervals of ~90 meV from the zero-phonon line, with DAP_2 showing a stronger phonon coupling due to the deeper acceptors involved, as expected. No luminescence at 3.48 eV, which is the excitonic recombination of h-GaN, is observed. A broad emission centered at 3.67 eV with an fwhm of 220 meV is reported. Injection current dependent CL is used to determine the nature of this radiative recombination center. A power-law study reveals a linear relationship between its intensity $\left(I_{CL}^{3.6\mathrm{eV}}\right)$ and injection current (J_b) with a slope of 0.9 ± 0.2, which indicates an unsaturated, band-to-band-like transition across the injection current range of 0.1 to 3.2 nA $\left(I_{\mathrm{CL}}^{3.67\mathrm{eV}} \propto J_{\mathrm{b}}^{0.9}\right)$.[40] Since the emission energy is above both cubic and hexagonal phase GaN, it is likely from neither crystal phases. We attribute this to the presence of the exposed AlN

nucleation layer on the SiO_2 sidewalls, considering the persistent AlN phonon shifts observed in Raman spectroscopy (Figure 3) across different *ff*'s.

Cathodoluminescence imaging was conducted to investigate the spatial distribution of the luminescence centers at 5.7 K. High-magnification SEM images of grooves with various *ff*'s from 30% to 205% are shown in Figure 8a, and a large-scale SEM image is shown in Figure 8b. The monochromatic CL images of the grooves shown in Figure 8b at λ = 355 nm (3.49 eV, h-GaN BX), 390 nm (3.18 eV, c-GaN DAP_1), and 420 nm (2.95 eV, c-GaN DAP_2) are shown in Figure 8c,d,e, respectively.

The luminescence of h-GaN BX (Figure 8c) in the undergrown U-grooves (*ff* = 30% and 40%) shows very uniform and intense luminescence, which indicates the presence of h-GaN on the surface, while the intermediate Ugrooves (*ff* = 65%, 70%, 90%) show a decreasing amount of luminescence at this energy, indicating the decreasing amount of h-GaN that is excited within the top ~47 nm layer. The most optimized U-grooves, *ff* = 95%, show no observable h-GaN emission, indicating a very good coverage of the c-GaN triangle on the surface. Beyond the optimized condition for phase transition at *ff* = 100%, traces of h-GaN BX luminescence can be observed scattered randomly across the image, indicating a reappearance of h-GaN in an irregular distribution. The luminescence of DAP_1 (Figure 8d) of c-GaN at 3.18 eV can be seen scattered randomly across the images in small and bright clusters. The intensity and concentration of these clusters seem to have a weak dependence on ff. At the extreme end of overgrowth (ff = 205%), the concentration of DAP_1 increases dramatically, but the cluster-like distribution persists. This suggests an increase in point defect formation (e.g., lattice site vacancies, V_{Ga}, V_N) or slip planes (e.g., basal stacking faults) rather than an extrinsic impurity (C, O, etc.) since the growth condition has not changed between the U-grooves. The formation of stacking faults is directly observed in Figure 3b near the c-GaN/oxide interface. The luminescence of c-DAP_2 (Figure 8e), while showing a similar cluster-like distribution observed in c-DAP_1, follows the trend of the cubic optimization. It is at its strongest when *ff* is the closest to 100% and becomes weaker as ff deviates from 100%. This suggests this luminescence center is unique to crystalline c-GaN and is not observed when a large degree of phase mixing or poor crystalline quality is present.

Temperature-dependent CL is conducted on c-GaN to calculate the energies of the donors and acceptors involved in DAP_1 and DAP_2. Figure 9 shows the Arrhenius plot of the integrated CL intensity of the three luminescence centers of cGaN. The integrated intensity obeys[41]

$$I(T) = \frac{I_0}{1 + C\exp\left(-E_{\text{act}}/k_{\text{B}}T\right)} \quad (5)$$

where I_0 and C are fitting constants, k_B is Boltzmann's constant, and T is the temperature. Fitting of the experimental data reveals a donor activation energy (E_{act}) of 20, 16, and 16 meV for BX (black squares), DAP_1 (violet circles), and DAP_2 (blue triangles), respectively. The activation energy for the bound exciton corresponds to the excitonic binding energy of

~20 meV. The similarity between the activation energies obtained for the DAPs implies these transitions involve the same shallow donor, which is believed to be silicon. Using the estimation of the shallow donor activation energy, the band gap of c-GaN at 0 K,[30] and the energies of the photon emitted, the calculated acceptor energies are 124 meV (DAP_1) and 344 meV (DAP_2). The shallow acceptor at 124 meV above the valence band is of particular interest, as it demonstrates the possibility of a much higher p-type doping efficiency and conductivity of c-GaN than that of h-GaN. A proposed band diagram of c-GaN is shown in the inset in Figure 9.

The internal quantum efficiency (IQE) provides insight into how efficient the radiative recombination process is compared to other nonradiative recombination mechanisms (e.g., Shockley–Reed–Hall, Auger) and how well these undesired carrier loss paths are suppressed in a photonic device. Using the results from the CL study, IQE of the band-to-band transition of h-GaN (3.48 eV) and c-GaN (3.28 eV) is calculated using[42]

$$\eta_{\mathrm{IQE}}(T) = \frac{I(T)}{I(5.7\mathrm{K})} \quad (6)$$

where $I(T)$ is the integrated intensity as a function of temperature and $\eta_{\mathrm{IQE}}(T)$ is the internal quantum efficiency, assuming the nonradiative recombination centers are fully deactivated at 5.7 K.[43] The estimated IQE for the optimized phase-transition c-GaN band-to-band transition is plotted as a function of temperature in Figure 10, which shows an IQE of 29% at room temperature.

The IQE value of 29% indicates phase transition and nanopatterning are capable of synthesizing crystals with excellent quality without the need for thick and intricate buffer layers. This is especially clear when compared to commercially available 3-μm-thick h-GaN on sapphire, 325-μm-thick HVPEgrown freestanding GaN, and GaN on Si(111), which exhibit IQE values of 12%, 8%, and 2%, respectively (see Supporting Information Figures S1, S2, S3).

The inset in Figure 10 shows the IQE of c-GaN for various ff from 0% (one h-GaN wing without any phase transition) to 210% (the U-grooves shown in the bottom row of Figure 7). The IQE for c-GaN increases very rapidly as *ff* approaches 100% and drops down to very small values once *ff* exceeds unity. IQE and CL imaging suggest the importance of U-pattern optimization and regrowth height. If GaN is under-deposited, c-GaN is unable to cover the entire surface, resulting in poor quantum efficiency. If GaN is over-deposited, defect formation dominates the material growth, resulting in poor quantum efficiency. There exists a relatively small window in which IQE is maximized for c-GaN crystals given a specific U-groove. This is when complete c-GaN coverage is achieved through eq 1.

Another approach to estimate τ_{rad} of c-GaN is to utilize the IQE calculated from eq 6. Using IQE = 29% and the measured τ_{PL} = 11 ps of c-GaN, the τ_{rad} can be extracted using eq 7. This yields a τ_{rad} of 38 ps, which is ~12.4 times shorter than the value for h-GaN, and a τ_{nr} of 22 ps. The finding in the TRPL for c-GaN is in good agreement with the other studies in the literature.[13,29] This method, which does not assume the relationship between the

radiative lifetime of c- and h-GaN, independently verifies the one-order faster radiative recombination lifetime in c-GaN than that of h-GaN observation.

$$\eta_{\mathrm{IQE}} = \frac{\tau_{\mathrm{PL}}}{\tau_{\mathrm{rad}}} \quad (7)$$

Fundamental material properties can be extracted using the observed radiative lifetime (38 ps) and eq 3. Assuming similar mass density and deformation potential between h-GaN and cGaN, the polarizability, α, can be calculated for c-GaN using the 3.22 eV for ω and 200 nm for L. The polarizability of c-GaN is calculated to be 8.3×10^{-11}, which is approximately 7 orders of magnitude smaller than that of h-GaN.

CONCLUSION

We demonstrate that phase transition of h-GaN to c-GaN is a reliable c-GaN growth technology that can be precisely controlled by substrate patterning and material growth. A high-crystallinity and -uniformity phase-transition c-GaN surface can be reproduced when the critical condition, $h_c = (1.06p - 0.75t_d)/(1 - \tan \alpha/0.71)$, is met. Phase-transition c-GaN is observed to be under tensile strain, and its light emission has 0.2 degree of polarization along the pattern direction. Low-temperature CL spectroscopy identified two defect luminescence centers at 144 and 344 eV above the valence band, and imaging of the distribution of these acceptors suggests these are intrinsic defect and extrinsic impurity levels, respectively. The band-to-band emission of phase-transition c-GaN internal quantum efficiency is calculated independently via temperature-dependent CL and time-resolved photoluminescence to be 29%, making this technology suitable for next-generation photonic devices.

Supplementary Material

Refer to Web version on PubMed Central for supplementary material.

ACKNOWLEDGMENTS

This work is supported by the National Science Foundation Faculty Early Career Development (CAREER) Program under award number NSF-ECCS-16–52871. R.L. acknowledges support from the NASA Space Technology Research Fellowship. Use of the Center for Nanoscale Materials, an Office of Science user facility, is supported by the U.S. Department of Energy, Office of Science, Office of Basic Energy Sciences, under Contract No. DE-AC02–06CH11357. The authors also acknowledge the UIUC-MRL seed project #8016 for structural microanalysis. This work was carried out in the Micro and Nanotechnology Laboratory and Frederick Seitz Materials Research Laboratory Central Research Facilities, University of Illinois at Urbana–Champaign, IL, USA. The authors acknowledge support from Dr. James Mabon and Dr. Julio Soares of University of Illinois at Urbana–Champaign, IL, USA.

REFERENCES

(1). Schubert EF; Kim JK; Luo H; Xi J-Q Solid-State Lighting–a Benevolent Technology. Rep. Prog. Phys 2006, 69, 3069–3099.

(2). Bernardini F; Fiorentini V; Vanderbilt D Spontaneous Polarization and Piezoelectric Constants of III-V Nitrides. Phys. Rev. B: Condens. Matter Mater. Phys 1997, 56, R10024–R10027.

(3). Uemoto Y; Hikita M; Ueno H; Matsuo H; Ishida H; Yanagihara M; Ueda T; Tanaka T; Ueda D Gate Injection Transistor (GIT) - A Normally-off AlGaN/GaN Power Transistor Using Conductivity Modulation. IEEE Trans. Electron Devices 2007, 54, 3393–3399.

(4). Zhao Y; Yan Q; Huang C-Y; Huang S-C; Shan Hsu P; Tanaka S; Pan C-C; Kawaguchi Y; Fujito K; Van de Walle CG; Speck JS; DenBaars SP; Nakamura S; Feezell D Indium Incorporation and Emission Properties of Nonpolar and Semipolar InGaN Quantum Wells. Appl. Phys. Lett 2012, 100, 201108.

(5). Xu S; Hao Y; Zhang J; Jiang T; Yang L; Lu X; Lin Z Yellow Luminescence of Polar and Nonpolar GaN Nanowires on RPlane Sapphire by Metal Organic Chemical Vapor Deposition. Nano Lett. 2013, 13, 3654–3657. [PubMed: 23899164]

(6). Paskova T; Kroeger R; Figge S; Hommel D; Darakchieva V; Monemar B; Preble E; Hanser A; Williams NM; Tutor M HighQuality Bulk a-Plane GaN Sliced from Boules in Comparison to Heteroepitaxially Grown Thick Films on R-Plane Sapphire. Appl. Phys. Lett 2006, 89, 1–4.

(7). Li S; Schörmann J; As DJ; Lischka K Room Temperature Green Light Emission from Nonpolar Cubic InGaNGaN Multi-Quantum-Wells. Appl. Phys. Lett 2007, 90, 10–13.

(8). Kim JG; Frenkel AC; Liu H; Park RM Growth by Molecular Beam Epitaxy and Electrical Characterization of Si-doped Zinc Blende GaN Films Deposited on β-SiC Coated (001) Si Substrates. Appl. Phys. Lett 1994, 65, 91–93.

(9). Brandt O; Yang H; Kostial H; Ploog KH High P -type Conductivity in Cubic GaN/GaAs(113) A by Using Be as the Acceptor and O as the Codopant. Appl. Phys. Lett 1996, 69, 2707–2709.

(10). Caetano EWS; Costa Filho RN; Freire VN; Da Costa JAP Velocity Overshoot in Zincblende and Wurtzite GaN. Solid State Commun. 1999, 110, 469–472.

(11). Delaney KT; Rinke P; Van De Walle CG Auger Recombination Rates in Nitrides from First Principles. Appl. Phys. Lett 2009, 94, 2007–2010.

(12). Kim C-H; Han B-H Valence Subbands and Optical Gain in Wurtzite and Zinc-Blende Strained GaN/AlGaN Quantum Wells. Solid State Commun. 1998, 106, 127–132.

(13). Simon J; Pelekanos NT; Adelmann C; Martinez-Guerrero E; Andre R; Daudin B; Dang LS; Mariette H Direct Comparison of Recombination Dynamics in Cubic and Hexagonal GaN/AlN Quantum Dots. Phys. Rev. B: Condens. Matter Mater. Phys 2003, 68, 35312.

(14). Lv B; Tang Y; Lou S; Xu Y; Zhou S Single P-N Homojunction White Light Emitting Diodes Based on High-Performance Yellow Luminescence of Large-Scale GaN Microcubes. J. Mater. Chem. C 2016, 4, 5416–5423.

(15). Auf Der Maur M; Pecchia A; Penazzi G; Rodrigues W; Di Carlo A Efficiency Drop in Green InGaN/GaN Light Emitting Diodes: The Role of Random Alloy Fluctuations. Phys. Rev. Lett 2016, 116, 27401.

(16). Kitamura T; Suzuki Y; Ishida Y; Shen XQ; Nakanishi H; Chichibu SF; Shimizu M Optical Properties of Cubic InGaN/GaN Multiple Quantum Wells on 3C-SiC Substrates by Radio-Frequency Plasma-Assisted Molecular Beam Epitaxy. Phys. Status Solidi a-Applied Res 2001, 188, 705–709.

(17). Compean García VD; Orozco Hinostroza IEE; Escobosá Echavarría A; Lopez Luna E; Rodríguez AG; Vidal MAA Bulḱ Lattice Parameter and Band Gap of Cubic InXGa1-XN (001) Alloys on MgO (100) Substrates. J. Cryst. Growth 2015, 418, 120–125.

(18). As DJ; Richter A; Busch J; Lübbers M; Mimkes J; Lischka K Electroluminescence of a Cubic GaN/GaAs (001) P–n Junction. Appl. Phys. Lett 2000, 76, 13–15.

(19). Chichibu SF; Onuma T; Aoyama T; Nakajima K; Ahmet P; Chikyow T; Sota T; DenBaars SP; Nakamura S; Kitamura T; Ishida Y; Okumura H Recombination Dynamics of Localized Excitons in Cubic In[sub x]Ga[sub 1–x]N/GaN Multiple Quantum Wells Grown by Radio Frequency Molecular Beam Epitaxy on 3C–SiC Substrate. J. Vac. Sci. Technol., B: Microelectron. Process. Phenom 2003, 21, 1856–1862.

(20). Kemper RM; Haberlen M; Schupp T; Weinl M; Bŭrger M; Ruth M; Meier C; Niendorf T; Maier HJ; Lischka K; As DJ; Lindner JKN Formation of Defects in Cubic GaN Grown on Nano-Patterned 3C-SiC (001). Phys. Status Solidi Curr. Top. Solid State Phys 2012, 9, 1028–1031.

(21). Lee SC; Sun XY; Hersee SD; Brueck SRJ; Xu H Spatial Phase Separation of GaN Selectively Grown on a Nanoscale Faceted Si Surface. Appl. Phys. Lett 2004, 84, 2079–2081.

(22). Lee SC; Youngblood N; Jiang YB; Peterson EJ; Stark CJM; Detchprohm T; Wetzel C; Brueck SRJ Incorporation of Indium on Cubic GaN Epitaxially Induced on a Nanofaceted Si(001) Substrate by Phase Transition. Appl. Phys. Lett 2015, 107, 1–6.

(23). Durniak MT; Bross AS; Elsaesser D; Chaudhuri A; Smith ML; Allerman AA; Lee SC; Brueck SRJ; Wetzel C Green Emitting Cubic GaInN/GaN Quantum Well Stripes on Micropatterned Si (001) and Their Strain Analysis. Adv. Electron. Mater. No 2016, 1, 1–8.

(24). Bayram C; Ott JA; Shiu K-TT; Cheng C-WW; Zhu Y; Kim J; Razeghi M; Sadana DK Cubic Phase GaN on Nano-Grooved Si (100) via Maskless Selective Area Epitaxy. Adv. Funct. Mater 2014, 24, 4492–4496.

(25). Liu R; Bayram C Maximizing Cubic Phase Gallium Nitride Surface Coverage on Nano-Patterned Silicon (100). Appl. Phys. Lett 2016, 109, 38–41.

(26). Siegle H; Eckey L; Hoffmann A; Thomsen C; Meyer BK; Schikora D; Hankeln M; Lischka K Quantitative Determination of Hexagonal Minority Phase in Cubic GaN Using Raman Spectroscopy. Solid State Commun. 1995, 96, 943–949.

(27). Bayram C; Shiu KT; Zhu Y; Cheng CW; Sadana DK; Teherani FH; Rogers DJ; Sandana VE; Bove P; Zhang Y; Gautier S; Cho C-Y; Cicek E; Vashaei Z; McClintock R; Razeghi M Engineering Future Light Emitting Diodes and Photovoltaics with Inexpensive Materials: Integrating ZnO and Si into GaN-Based Devices. In Proc. SPIE; Teherani FH, Look DC, Rogers DJ, Eds.; 2013; Vol. 8626, p 86260L1–12.

(28). Toyozawa Y On the Dynamical Behavior of an Exciton. Prog. Theor. Phys. Suppl 1959, 12, 111–140.

(29). Fonoberov VA; Balandin AA Excitonic Properties of Strained Wurtzite and Zinc-Blende GaN/Al xGa 1-xN Quantum Dots. J. Appl. Phys 2003, 94, 7178–7186.

(30). Liu R; Bayram C Cathodoluminescence Study of Luminescence Centers in Hexagonal and Cubic Phase GaN Hetero-Integrated on Si(100). J. Appl. Phys 2016, 120, 25106.

(31). Chichibu SF; Marchand H; Minsky MS; Keller S; Fini PT; Ibbetson JP; Fleischer SB; Speck JS; Bowers JE; Hu E; Mishra UK; DenBaars SP; Deguchi T; Sota T; Nakamura S Emission Mechanisms of Bulk GaN and InGaN Quantum Wells Prepared by Lateral Epitaxial Overgrowth. Appl. Phys. Lett 1999, 74, 1460–1462.

(32). Ki Kwon H; Eiting C; Lambert DJ; Wong M; Shelton B; Zhu T; Liliental-Weber Z; Benamura M; Dupuis R Time-Resolved Photoluminescence Study of GaN Grown by Metalorganic Chemical Vapor Deposition. J. Cryst. Growth 2000, 221, 240–245.

(33). Bunea GE; Herzog WD; Unlu MS; Goldberg BB; Molnar RJ Time-Resolved Photoluminescence Studies of Free and Donor-Bound Exciton in GaN Grown by Hydride Vapor Phase Epitaxy. Appl. Phys. Lett 1999, 75, 838–840.

(34). Chichibu SF; Uedono A; Onuma T; Sota T; Haskell BA; DenBaars SP; Speck JS; Nakamura S Limiting Factors of Room-Temperature Nonradiative Photoluminescence Lifetime in Polar and Nonpolar GaN Studied by Time-Resolved Photoluminescence and Slow Positron Annihilation Techniques. Appl. Phys. Lett 2005, 86, 21914.

(35). Church SA; Hammersley S; Mitchell PW; Kappers MJ; Sahonta SL; Frentrup M; Nilsson D; Ward PJ; Shaw LJ; Wallis DJ; Humphreys CJ; Oliver RA; Binks DJ; Dawson P Photoluminescence Studies of Cubic GaN Epilayers. Phys. Phys. Status Solidi B 2017, 254, 1600733.

(36). Athanasiou M; Smith RM; Ghataora S; Wang T Polarized White Light from Hybrid organic/III-Nitrides Grating Structures. Sci. Rep 2017, 7, 39677. [PubMed: 28045123]

(37). Feneberg M; Lipski F; Sauer R; Thonke K; Brückner P; Neubert B; Wunderer T; Scholz F Polarized Light Emission from Semipolar GaInN Quantum Wells on {11¯01} GaN Facets. J. Appl. Phys 2007, 101, 53530.

(38). Zhuang Z; Li Y; Liu B; Guo X; Dai J; Zhang G; Tao T; Zhi T; Xie Z; Ge H; Shi Y; Zheng Y; Zhang R Optical Polarization Characteristics of c -Plane InGaN/GaN Asymmetric Nanostructures. J. Appl. Phys 2015, 118, 233111.

(39). Kanaya KK; Okayama S Energy-Loss Theory of Electrons in Solid Targets. J. Phys. D: Appl. Phys 1972, 5, 43–58.

(40). Grieshaber W; Schubert EF; Goepfert ID; Karlicek RF; Schurman MJ; Tran C Competition between Band Gap and Yellow Luminescence in GaN and Its Relevance for Optoelectronic Devices. J. Appl. Phys 1996, 80, 4615–4620.

(41). Krustok J; Collan H; Hjelt K Does the Low-Temperature Arrhenius Plot of the Photoluminescence Intensity in CdTe Point towards an Erroneous Activation Energy? J. Appl. Phys 1997, 81, 1442–1445.

(42). Sasaki A; Shibakawa S; Kawakami Y; Nishizuka K; Narukawa Y; Mukai T Equation for Internal Quantum Efficiency and Its Temperature Dependence of Luminescence, and Application to In X Ga 1- X N/GaN Multiple Quantum Wells. Jpn. J. Appl. Phys 2006, 45, 8719–8723.

(43). Narukawa Y; Kawakami Y; Fujita S; Nakamura S Dimensionality of Excitons in Laser-Diode Structures Composed of InxGa1-xN Multiple Quantum Wells. Phys. Rev. B: Condens. Matter Mater. Phys 1999, 59, 10283–10288.

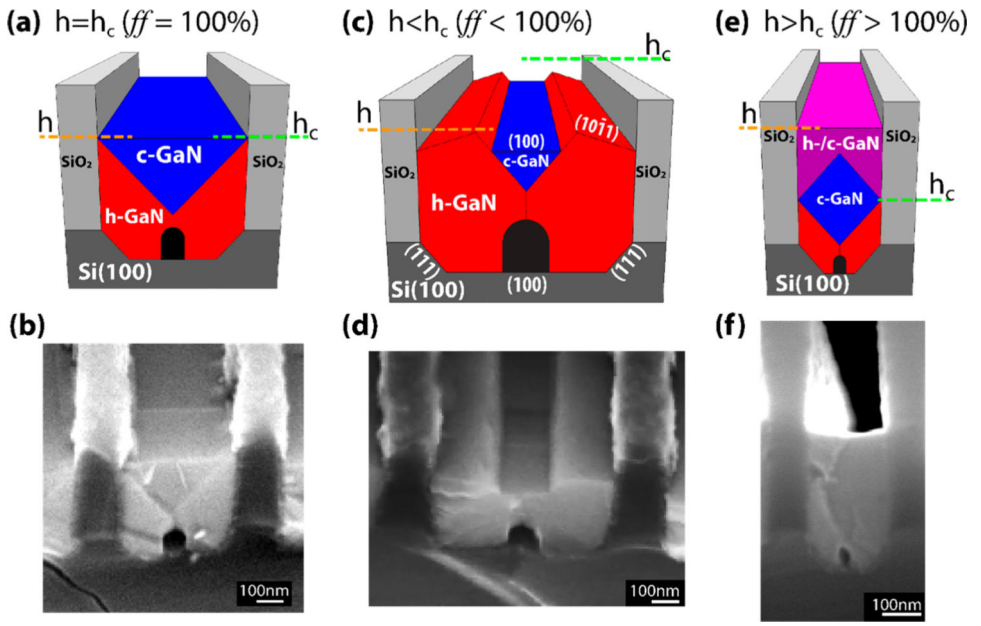

Figure 1.

Phase-transition GaN drawings (a, c, e) and SEMs (b, d, f) under various conditions. In (a) and (b), the U-groove is optimized ($h = h_c$), enabling complete c-GaN (blue) surface coverage. In (c) and (d), the U-groove is underdeposited ($h < h_c$), leading to a dual-phase surface of c-GaN (blue) flanked by h-GaN $(10\bar{1}1)$ planes (red). In (e) and (f), the U-groove is overdeposited ($h > h_c$), resulting in a defective, mixed phase material (purple).

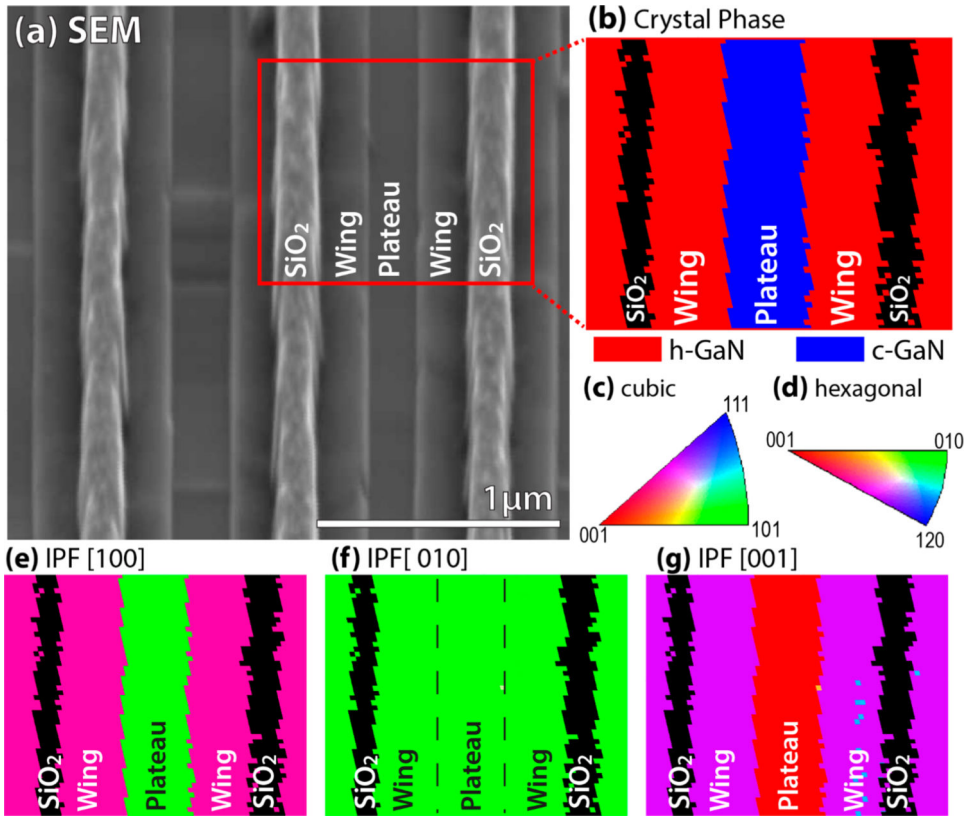

Figure 2.

EBSD investigation showing the orientation of c- and h-GaN. (a) Top-view SEM of the underdeposited GaN leading to a dual-phase surface of c-GaN flanked by h-GaN planes. (b) EBSD phase detection of the region marked by the red box. Color key for (c) cubic and (d) hexagonal crystal inverse pole figures in the (e) [100], (f) [010], and (g) [001] directions. Each pixel is 20 × 20 nm.

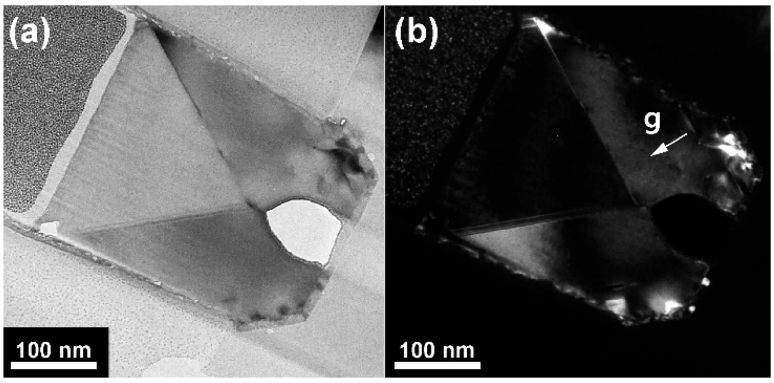

Figure 3.

TEM images of GaN crystals in a U-groove. (a) Bright field and (b) dark field image taken at g = 0002 near the $[1\bar{2}10]$ zone axis of the right-side h-GaN.

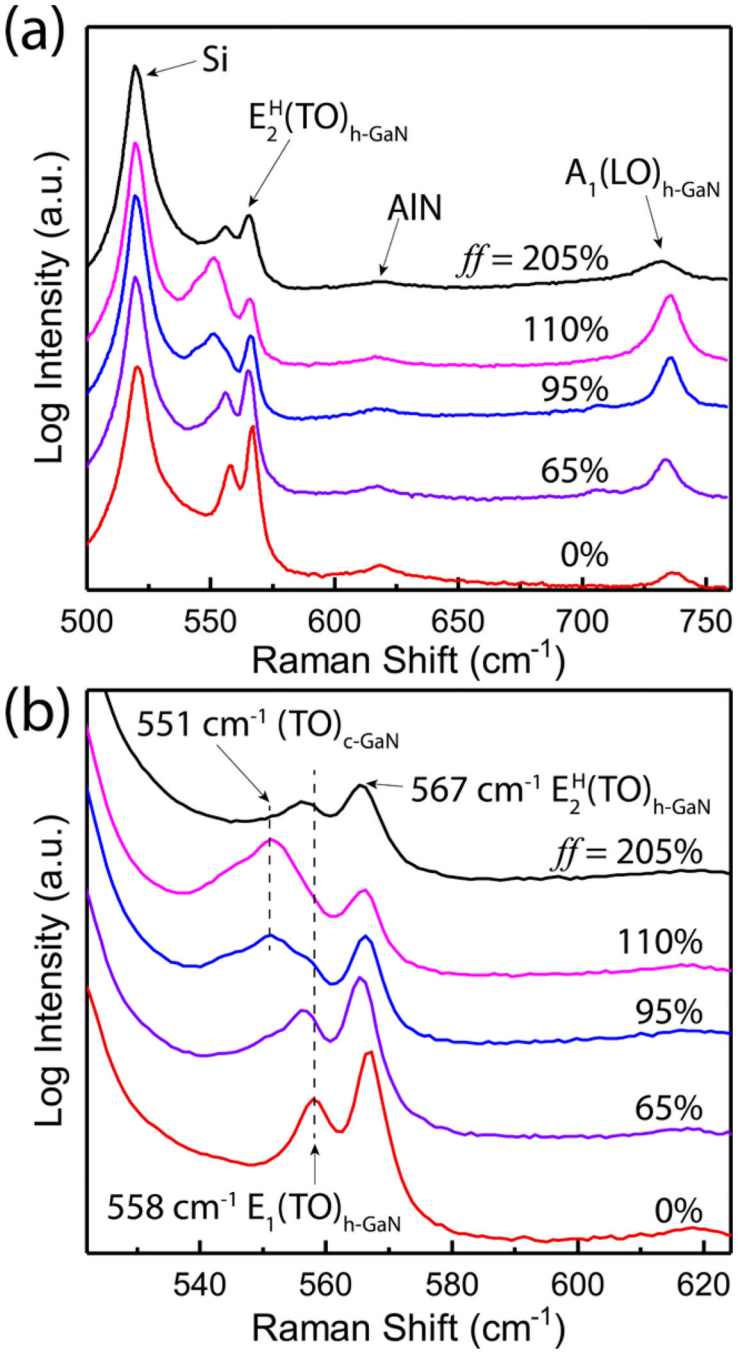

Figure 4.

Confocal Raman spectroscopy of U-grooves with ff 's from 0% (purely h-GaN) to 210% (overgrown-mixed phase GaN). In (a), four peaks are labeled: $A_1(LO)$ and $E_2^H(TO)$ of h-GaN, Si, and $A_1(LO)$ of the AlN nucleation layer. In (b), as phase transition occurs, c-GaN's TO-phonons can be observed. At ff = 205%, the extremely overdeposited case, c-GaN's TO-phonon disappears, and the fwhm of h-GaN's signal increases, indicating a reduction in crystallinity.

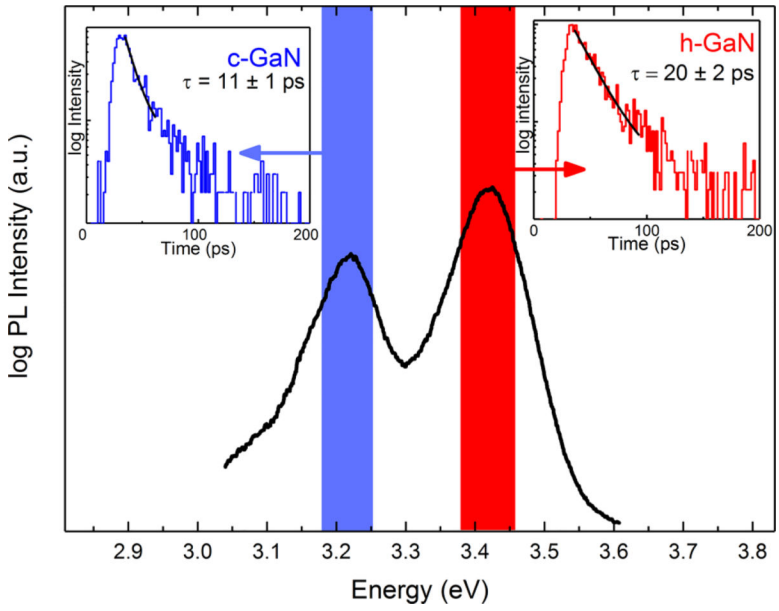

Figure 5.

Room-temperature PL spectra of the U-grooves. Near band edge emissions of h-GaN at 3.42 eV (red) and c-GaN at 3.22 eV (blue) are observed. The time-resolved PL luminescence decay of the marked spectral ranges are shown as insets.

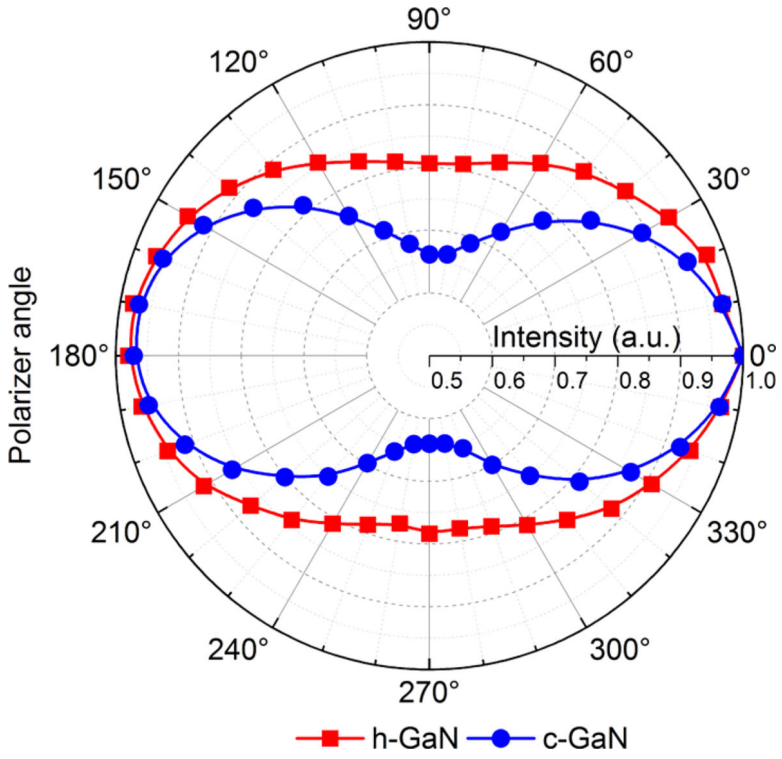

Figure 6.

Polarization-dependent photoluminescence of the near band edge emission of h-GaN (red squares) and c-GaN (blue circles). The passing axis of the polarizer angle is parallel to the direction of the Ugrooves. The minimum occurs when the polaroid is 90° to the direction of grooves for both materials, with c-GaN showing a higher degree of polarization than h-GaN.

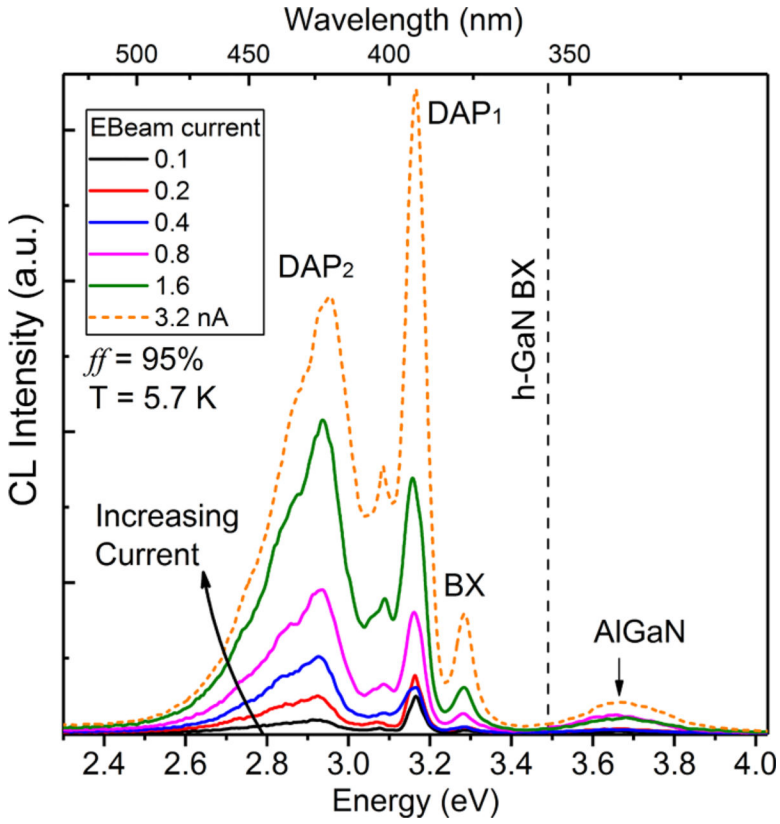

Figure 7.

Low-temperature CL spectra of the c-GaN. Bound exciton (BX) at 3.28 eV, two donor–acceptor pairs at 3.18 (DAP_1) and 2.95 (DAP_2) eV, as well as their LO-phonon replicas, of c-GaN are observed. A band-to-band-like emission at 3.67 eV with fwhm = 220 meV is also observed. No h-GaN emission at 3.48 eV (vertical dashed line) is detected, indicating no h-GaN incursions.

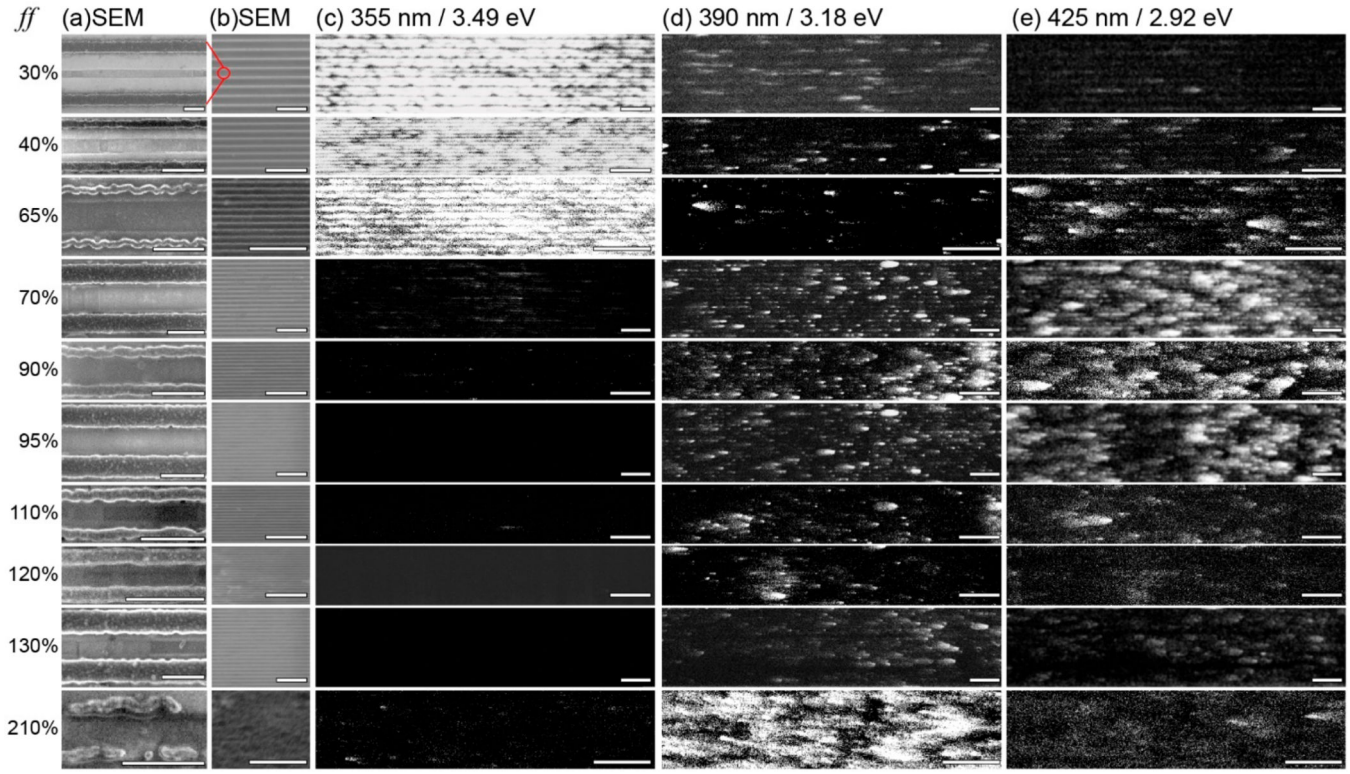

Figure 8.

Plain view SEM and CL images of GaN on various U-grooves. (a) High-magnification SEM images with a scale bar of 500 nm. (b) Lowmagnification SEM image with scale bars of 5 μm, and its corresponding monochromatic CL images at (c) the band gap of h-GaN at 355 nm, (d) DAP_1 of c-GaN at 390 nm, and (e) DAP_2 of c-GaN at 425 nm.

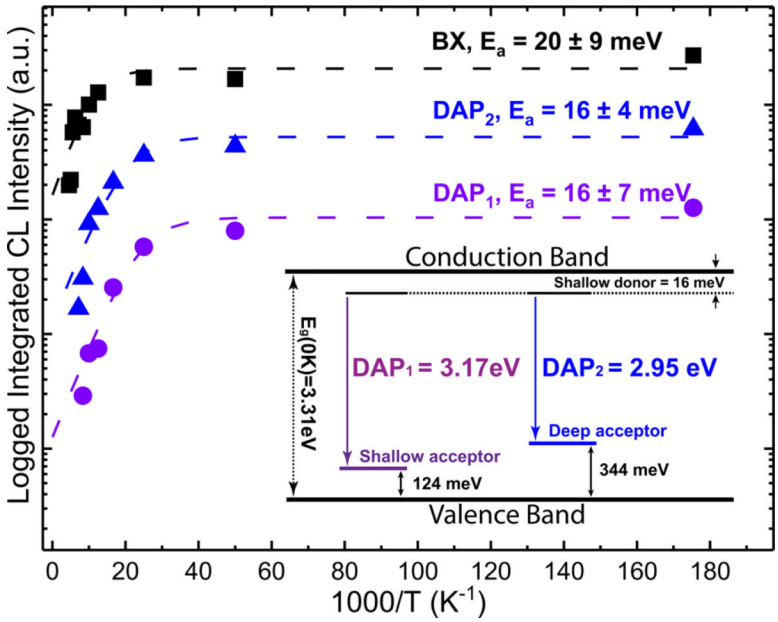

Figure 9.

Arrhenius plot of c-GaN CL emissions at 5.7 K. Fitting shows an activation energy of 20 ± 9, 16 ± 7, and 16 ± 4 meV for BX (exciton binding energy), DAP_1 (shallow donor), and DAP_2 (shallow donor), respectively. The proposed band diagram for each radiative recombination is shown as the inset.

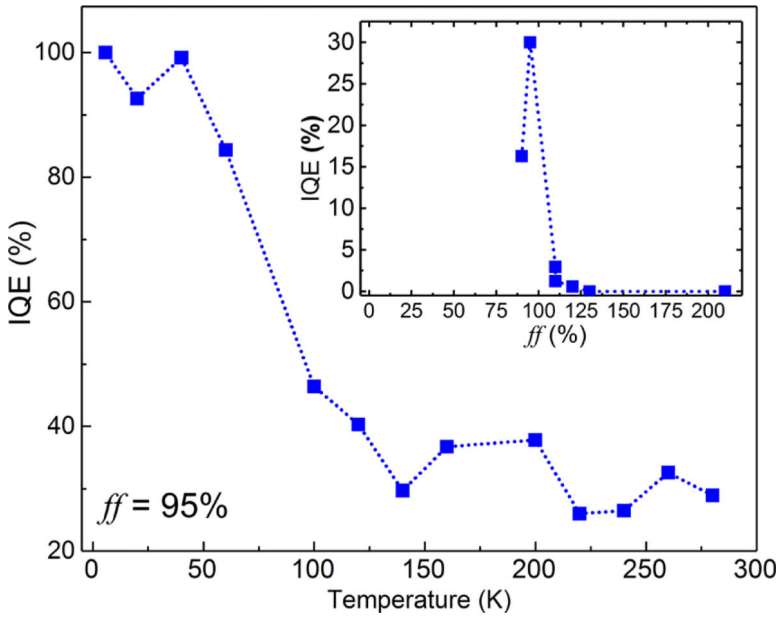

Figure 10.

Temperature dependence of c-GaN IQE. Room-temperature IQE of c-GaN with various values of *ff* are shown in the inset. The highest c-GaN IQE is achieved when *ff* ≈ 95%, and its temperature dependence is also shown.